Delay of the First Transition of Asian Summer Monsoon under Global Warming Condition

Tomoshige Inoue and Hiroaki Ueda
Graduate School of Life and Environmental Sciences, University of Tsukuba, Tsukuba, Japan

Abstract

We evaluate reproducibility of seasonal evolution of the thermal fields associated with the first transition of Asian summer monsoon (ASM) in atmosphere-ocean coupled general circulation models (CGCMs) of the Coupled Model Intercomparison Project phase 3 (CMIP3). Many CGCMs reproduce seasonal evolution of the thermal fields related to the first transition of ASM well, though the degree of reproducibility differs to some extent. Based on this evaluation, weighted multi-model ensembles are calculated, and the future projections of the ASM onset from the viewpoint of lower-tropospheric westerlies are conducted. The onset dates over the Bay of Bengal, the Indochina Peninsula and the South China Sea are projected to delay by 5 to 10 days in the end of the 21st century under the A1B scenario of the Special Report on Emission Scenarios (SRES), compared to those in the end of the 20th century. This change might be related with delay of the reversal of upper-tropospheric meridional thermal gradient between over the Eurasian Continent and the north Indian Ocean.

1. Introduction

The Asian summer monsoon (ASM) is one of the most important components in the global climate system, providing an enormous amount of water resources over the most densely populated regions of the world. The ASM exhibits three-time stepwise seasonal evolutions occurring in mid-May (the first transition; Lau et al. 1998), mid-June (mature stage of ITCZ; Murakami and Matsumoto 1994) and mid-July (convection jump; Ueda et al. 1995). Among these, the physical processes involved in the mid-May change bear considerable resemblance with the establishment and maintenance of ASM (Li and Yanai 1996). In mid-May, reversal of meridional thermal gradient in the upper troposphere between the Asiatic landmass and the tropics takes place, which is concurrent with acceleration of monsoon westerlies in the lower troposphere extending over the Bay of Bengal through the western North Pacific (WNP). Associated with the eastward intrusion of monsoon westerlies toward WNP, the tropical easterlies to the east of the Philippines become weak, which is responsible for sea surface temperature (SST) warming and subsequent enhancement of ocean convection (Ueda 2005). Given these, the timing of the eastward penetration of low-level monsoon westerlies relevant to the modulation of the meridional thermal gradient is an important factor for the understanding of ASM as well as WNP monsoon. Therefore here arises a question, if such changes could be seen in transient 21st century experiments.

Recent assessment results for the future projections are summarized in the Fourth Assessment Report (AR4) of the Intergovernmental Panel on Climate Change (IPCC), based on multi-model outputs by atmosphere-ocean coupled general circulation models (CGCMs) from many climate research centers and institutes of the world which participate in the World Climate Research Programme's Coupled Model Intercomparison Project phase 3 (CMIP3; Meehl et al. 2007). Reproducibility of seasonal evolution of ASM in the CMIP3 CGCMs is evaluated by some studies (e.g., Inoue and Ueda 2009; Li and Zhang 2009). On the future projections of the seasonal evolutions of ASM based on these CGCMs, Kitoh and Uchiyama (2006) examined the changes in onset and withdrawal of the monsoon based on precipitation data. It is interesting to know how future changes of the monsoon circulation are associated with the modulation of the seasonal evolutions of ASM which has been shown by Kitoh and Uchiyama (2006). In the present study, we evaluate reproducibility of seasonal evolution of large-scale upper-tropospheric thermal fields associated with the first transition of ASM in mid-May. Based on the reproducibility, weighted multi-model ensembles are calculated, and future projections of ASM onset from the viewpoint of lower-tropospheric westerlies are examined. Section 2 describes data utilized in the present study. Results and discussion are shown in Section 3, and a brief summary is given in Section 4.

Corresponding author: Tomoshige Inoue, Graduate School of Life and Environmental Sciences, University of Tsukuba, 1-1-1 Tennodai, Tsukuba, Ibaraki 305-8572, Japan. E-mail: t-inoue@envr.tsukuba.ac.jp.

2. Data

As listed in Table 1, we analyze daily wind data under the 20th Century Climate in Coupled Models (20C3M) and Special Report on Emission Scenarios (SRES) A1B experiments from 19 CMIP3 CGCMs. Among the SRES's scenarios, the number of available CGCM outputs is largest under the SRES-A1B scenario, thus we examine the result of SRES-A1B for future projection. Details of these CGCMs are documented on the web site (http://www-pcmdi.llnl.gov/ipcc/about_ipcc.php) at the Program for Climate Model Diagnosis and Intercomparison (PCMDI). To calculate multi-model ensembles, data are interpolated into the common 2.5° by 2.5° horizontal grids. In order to equally treat each CGCM, only the first member of simulation is used in the present study, even if multi-member output is available for several CGCMs. Climatological means for each of the model outputs are defined as averages for 19-year periods of the end of the 20th and the 21st centuries (i.e., 1981−99 for 20C3M, and 2081−99 for SRES-A1B). In order to evaluate each CGCM's reproducibility, we use the 40-year Reanalysis from the European Centre for Medium-Range Weather Forecasts (ERA-40; Uppala et al. 2005). Also in this dataset, 19-year (1981−99) averages are used for comparison.

3. Results and discussion

Observational studies (Li and Yanai 1996; Ueda and Yasunari 1998) have revealed that the first transition of ASM occurs in mid-

Table 1. List of CGCMs used in the present study.

ID	Model acronym	ID	Model acronym
A	BCCR-CM2.0	K	FGOALS-g1.0
B	CGCM3.1 (T47)	L	INGV-ECHAM4
C	CGCM3.1 (T63)	M	INM-CM3.0
D	CNRM-CM3	N	IPSL-CM4
E	CSIRO-MK3.0	O	MIROC3.2 (hires)
F	CSIRO-MK3.5	P	MIROC3.2 (medres)
G	GFDL-CM2.0	Q	ECHO-G
H	GFDL-CM2.1	R	ECHAM5/MPI-OM
I	GISS-AOM	S	MRI-CGCM2.3.2
J	GISS-ER		

May, when upper-tropospheric meridional thermal gradient between over the northern Indian Ocean and the Eurasian Continent reversed. Thus in the present study, we compare reproducibility of the seasonal evolution of upper-tropospheric thermal fields between observation and each model. Lower-tropospheric wind is not directly compared here, since there are some difficulties such as treatment of topography due to different original grid spacing in the CGCMs. Previous studies such as Kawamura (1998) compared thickness between 200 hPa and 500 hPa as the thermal fields, but daily data of geopotential height are not available in most of the CMIP3 CGCMs. Instead, we analyze 300 hPa temperature fields. Spatial patterns of the 300 hPa temperature changes at mid-May (30-day average from 16-May to 14-June minus that from 16-April to 15-May) in observations and 20C3M experiment (climatological means of 1981−99) of the CMIP3 CGCMs are presented in a supplement figure (Fig. S1). In observation, a center of the temperature increase is observed over the southern periphery of the Tibetan Plateau and its vicinity. Many CGCMs reproduce this pattern well in general, but the center of the temperature increase is not consistent with observations in some CGCMs.

In order to quantitatively evaluate the reproducibility, we calculate Taylor's skill score about the upper-tropospheric patterns over a large-area of ASM region (30°E−140°E, 0°N−50°N). Taylor (2001) proposed the following skill score (S) for evaluation:

$$S = \frac{4(1+R)^4}{\left(SDR + \frac{1}{SDR}\right)^2 (1+R_0)^4}, \quad (1)$$

where R is a spatial correlation coefficient between each CGCM and the observations (ERA-40 in the present study), SDR is a ratio of spatial standard deviations for each model against observations, and R_0 is a maximum correlation coefficient attainable between intra-ensemble members in the same model. We assume R_0 as unity, since only the first member of simulation is used in the present study. Table 2 shows the skill scores (S) of the seasonal change patterns. The scores range from 0.26 to 0.85. To visualize the performances of the respective CGCMs clearly, a Taylor diagram (Taylor 2001) for the spatial patterns of the seasonal temperature change is shown in Fig. 1. This diagram is widely used for evaluation of models' performance with respect to observations. In this diagram, a reference dataset (Obs.) is plotted along the abscissa. The spatial correlation between each CGCM and observation is related to the azimuthal angle, and the radial distance from the origin indicates the standard deviation. The distance between each CGCM and a reference dataset is proportional to the root-mean-square error after the removal of the spatial average. In many CGCMs, radial distances from the origin are close to those of the observations, and correlation coefficients range 0.7−0.9. But there are some CGCMs whose scores are not so high. For example, score of model N is low because the temperature increase over the Eurasian Continent is not obvious (see Fig. S1). Since the reproducibility of the seasonal temperature fields differ from model to model, we calculate weighted multi-model ensembles (w-MME hereafter) of 19-year mean daily 850 hPa zonal wind in 20C3M and SRES-A1B, where weighting factors of the CGCMs are proportional to S. Then, onset dates of w-MME of both 20C3M and SRES-A1B are determined as the first days when 850 hPa zonal wind of w-MME changes from easterly to westerly at each 2.5° by 2.5° horizontal grid in March−July.

Table 2. Taylor's skill scores (S) for the seasonal change of 300 hPa temperature in middle May (30-day average from 16-May to 14-June minus that from 16-April to 15-May) over the ASM region (30°E−140°E, 0N°−50°N) for the period 1981−99 (20C3M) in each CGCM. Model IDs are listed in Table 1.

ID	S	ID	S	ID	S	ID	S
A	0.755	F	0.798	K	0.636	P	0.751
B	0.773	G	0.718	L	0.619	Q	0.507
C	0.833	H	0.748	M	0.655	R	0.804
D	0.655	I	0.526	N	0.260	S	0.591
E	0.457	J	0.508	O	0.847		

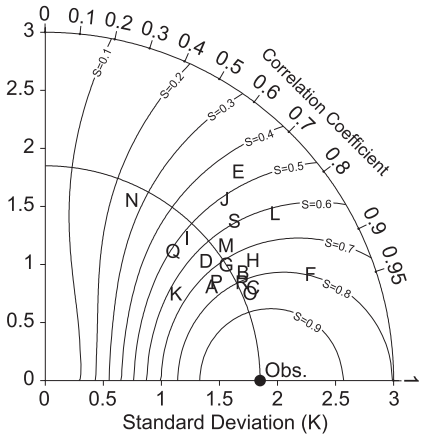

Fig. 1. Taylor diagram for the seasonal change of 300 hPa temperature in middle May (30-day average from 16-May to 14-June minus that from 16-April to 15-May) over the ASM region (30°E−140°E, 0°N−50°N) for the period 1981−99 (20C3M) in each CGCM. Letters indicate model IDs shown in Table 1.

Figure 2 shows the onset dates of ASM in observations, and 20C3M based on w-MME. The onset dates based on w-MME correspond well with those in observations over the northern Indian Ocean and the South China Sea, where onset occurs prior to mid-May. After mid-May, on the other hand, there is discrepancy of eastward advance of lower-tropospheric westerlies between observations and w-MME. In observations, two stepwise expansions of onset (early June around 5°N, 125°E and middle July around 12.5°N, 135°E) are recognized, whereas the eastward expansions are contiguous rather than stepwise in w-MME. This tendency is similar to our previous study (Inoue and Ueda 2009) based on precipitation data.

Figure 3 shows differences of ASM onset dates and their inter-model consistency between 20C3M (1981−99) and SRES-A1B (2081−99) based on w-MME. The most obvious change is a delay of the onset by 5−10 days in the Bay of Bengal, the vicinity of the Malay Peninsula, and the South China Sea, where the climatological onset occurs in late April to May (Fig. 2). Especially, the onset dates are projected to delay by more than 10 days in the southern

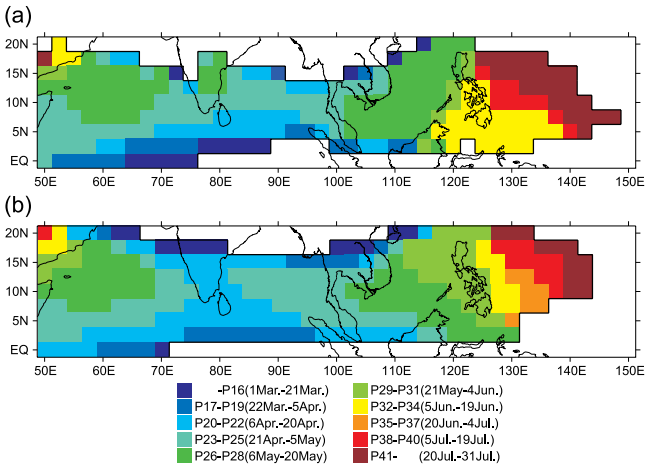

Fig. 2. Climatological onset dates of 850 hPa westerlies in (a) observational dataset (ERA-40) and (b) w-MME of 20C3M. Color shading (white) area denotes that the onset dates can (cannot) be defined (i.e., climatological 850 hPa zonal wind changes from easterlies to westerlies during March−July).

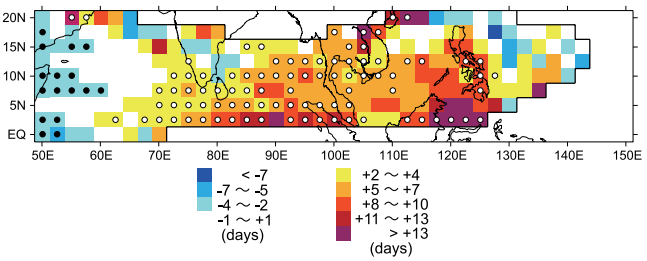

Fig. 3. Differences of the onset dates of 850 hPa westerlies between 20C3M (1981−99) and SRES-A1B (2081−99) based on w-MME (SRES-A1B minus 20C3M). Blue (Red) grids indicate that the onset dates become earlier (later). The onset dates in both 20C3M and SRES-A1B can be defined on the inside of the black solid lines. Open (Filled) circles means that the change is consistent in more than two-thirds (66.7%) of the CGCMs.

part of the South China Sea. Inter-model consistency is high over the Bay of Bengal and its vicinity. Over the western Arabian Sea, many CGCMs project that the westerlies will start earlier, though the differences of dates are not large. Over the WNP to the east of the Philippines, positive and negative grids are mixed, exhibiting spatially inhomogeneous features. This implies that, in the CGCMs, the monsoon onset over WNP is not directly influenced by the delay of the first transition in mid-May. In many CGCMs, however, convections over the WNP tend to start under a lower in situ SST than that in observations (Inoue and Ueda 2009), suggesting that the reproduction of the seasonal evolution of the WNP monsoon is still fundamental challenging topic in the state-of-the-art CGCMs (Wang et al. 2005).

The delay of the onset over the Bay of Bengal and the South China Sea might be associated with change in large-scale circulations and thermal fields under global warming situations. Also in w-MME, seasonal temperature increase in mid-May of 20C3M is most obvious over the Eurasian Continent (Fig. 4a). Figure 4b shows differences of 300 hPa temperature in May between 20C3M (1981−99) and SRES-A1B (2081−99) based on w-MME. Upper tropospheric temperature is projected to rise larger over the equatorial Indian Ocean, compared with that over the Eurasian Continent. This tendency is similar to the result in JJA mean field by Ueda et al. (2006). Figure 5a compares seasonal evolutions of upper-tropospheric MTG in 20C3M and SRES-A1B. Here, MTG is defined as area-averaged 300 hPa temperature differences between over the continent (20°N−40°N, 50°E−100°E) and northern Indian Ocean (0°N−20°N, 50°E−100°E), which is similar to an index by Kawamura (1998). In both periods, the northward negative MTG values change into positive as the season advances from boreal winter to summer. However, the MTG values in SRES-A1B are lower than those in 20C3M throughout the period. From a viewpoint of the seasonal changes, the MTG in SRES-A1B delays by 5−10 days compared with that in 20C3M. As expected from thermal wind relationship, development of the upper tropospheric easterlies over the tropics also delay (figure not shown). Figure 5b

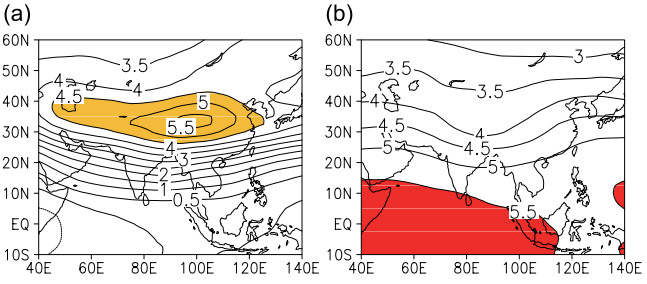

Fig. 4. (a) Seasonal change (16May−14Jun. minus 16Apr.−15May) of 300 hPa temperature in 20C3M based on w-MME. Temperature increase more than 4.5 K is shaded. (b) Difference of 300 hPa temperature in May between 20C3M (1981−99) and SRES-A1B (2081−99) based on w-MME (SRES-A1B minus 20C3M). Shading denotes regions where the warming is more than 5.5 K.

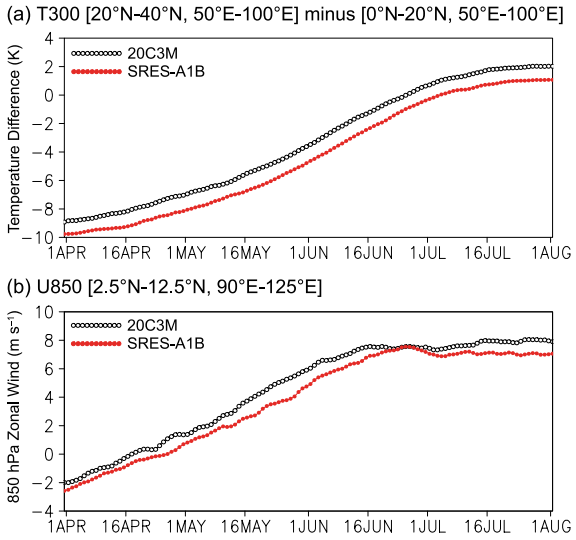

Fig. 5. Seasonal evolutions of (a) 300 hPa temperature differences ([average of 20°N−40°N, 50°E−100°E] minus [average of 0°N−20°N, 50°E−100°E]), and (b) 850 hPa zonal wind averaged over 2.5°N−12.5°N, 90°E−125°E, in 20C3M (open circles) and SRES-A1B (filled red circles) based on w-MME.

shows seasonal changes of 850 hPa zonal wind over the southern part of the Bay of Bengal and the South China Sea (2.5°N−12.5°N, 90°E−125°E) where the delay is most obvious in Fig. 3. As with MTG, development of lower tropospheric westerlies also delays by 5−10 days.

Richter and Xie (2008) showed that the larger warming in the upper troposphere over the tropics are also recognized in annual mean field, and mentioned that this is a result from the fact that the tropical atmosphere tends to maintain a moist adiabatic lapse rate (Xu and Emanuel 1989), even under global warming (Santer et al. 2005). The first transition of ASM in mid-May occurs concurrently with the upper-tropospheric change in thermal condition (e.g., Li and Yanai 1996), which is associated with the upper-tropospheric tropical easterlies to the south of the center of temperature increase (Fig. 4a). Since the upper-tropospheric easterlies are well correlated with low-level monsoon westerlies (Webster and Yang 1992), the delayed development of upper-tropospheric easterlies under global warming situation might be related with the delay of the onset of the lower-tropospheric westerlies over the Bay of Bengal and the South China Sea.

In order to investigate robustness of these changes among the CGCMs, Fig. 6 shows differences (SRES-A1B minus 20C3M) of MTG and 850 hPa zonal wind over the southern part of the Bay of Bengal and the South China Sea in May by each CGCM and w-MME. Negative MTG values are recognized in all CGCMs. The difference between 20C3M and SRES-A1B is statistically significant at 95% level according to the Student's t-test, when the 19-year mean value of the CGCMs is regarded as independent each other. Lower-tropospheric westerlies are projected to become weak in 14 out of the 19 CGCMs, though the difference is not statistically significant according to the Student's t-test. Even in the CGCMs which show stronger westerlies after global warming, the absolute difference values are small, thus the westerlies will become weak in w-MME. From this result, the delay of the onset is considerably robust.

Kitoh and Uchiyama (2006) investigated future projection of ASM onset based on precipitation data. They showed the onset date over the Indochina Peninsula and its vicinity is projected to delay (in their Fig. 4). The present results are consistent with the result by Kitoh and Uchiyama (2006), and the delay of the first transition of large-scale ASM circulations might cause delayed start of rainfall over there. Meanwhile, delay of monsoon westerlies is also recognized where the onset occurs before the first transition in mid-May (Figs. 2 and 3). The start of low-level westerlies

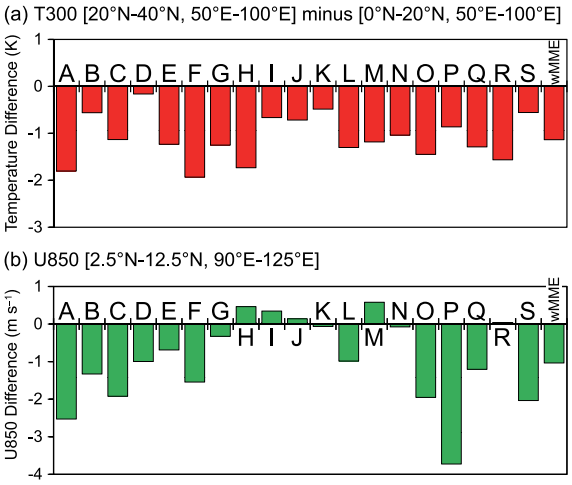

Fig. 6. Differences (SRES-A1B minus 20C3M) of (a) 300 hPa temperature differences (average of 20°N−40°N, 50°E−100°E minus average of 0°N−20°N, 50°E−100°E), and (b) 850 hPa zonal wind averaged over 2.5°N−12.5°N, 90°E−125°E in May. Alphabet letters indicate model IDs in Table 1, and rightmost bars are based on w-MME.

near the equator over the Indian Ocean does not seem to be related with the upper-tropospheric change, and further studies might be needed in order to explain the reason for the delay.

4. Summary

Reproducibility of seasonal evolution of the thermal fields in the first transition of ASM in the CMIP3 CGCMs is evaluated. Many CGCMs reproduce seasonal evolution of the thermal fields related to the first transition of ASM well, though the degree of reproducibility differs to some extent. Based on this evaluation result, weighted multi-model ensembles are calculated, and the future projections of the ASM onset from the viewpoint of lower-tropospheric westerlies are conducted. As a result, the onset dates over the Bay of Bengal, the Indochina Peninsula and the South China Sea are projected to delay by 5 to 10 days in the end of the 21st century under SRES-A1B scenario compared to those in the end of the last century. This change might be related with delay of the reversal of upper-tropospheric meridional thermal gradient between over the Eurasian Continent and the north Indian Ocean.

Acknowledgements

We thank the editor and anonymous reviewers for their valuable comments that helped us to improve our manuscript. This work is supported by the Global Environment Research Fund (S-5-2) of the Ministry of the Environment, Japan. We acknowledge the modeling groups, the Program for Climate Model Diagnosis and Intercomparison (PCMDI) and the WCRP's Working Group on Coupled Modelling (WGCM) for their roles in making available the WCRP CMIP3 multi-model dataset. Support of this dataset is provided by the Office of Science, U.S. Department of Energy. We also express our gratitude to the "Data Integration and Analysis System (DIAS)" Fund for National Key Technology from the Ministry of Education, Culture, Sports, Science and Technology, Japan, for providing us with an invaluable environment for a mass data handling.

Supplement

Figure S1 shows spatial patterns of seasonal change in mid-May (16May−14June minus 16April−15May) of 300 hPa temperature in observation (ERA-40) and the respective CGCMs.

References

Inoue, T., and H. Ueda, 2009: Evaluation for the seasonal evolution of the summer monsoon over the Asian and western North Pacific sector in the WCRP CMIP3 multi-model experiments. *J. Meteor. Soc. Japan*, **87**, 539−560.

Kawamura, R., 1998: A possible mechanism of the Asian summer monsoon-ENSO coupling. *J. Meteor. Soc. Japan*, **76**, 1009−1027.

Kitoh, A., and T. Uchiyama, 2006: Changes in onset and withdrawal of the East Asian summer rainy season by multi-model global warming experiments. *J. Meteor. Soc. Japan*, **84**, 247−258.

Lau, K.-M., H.-T. Wu, and S. Yang, 1998: Hydrologic processes associated with the first transition of the Asian summer monsoon: A pilot satellite study. *Bull. Amer. Meteor. Soc.*, **79**, 1871−1882.

Li, C., and M. Yanai, 1996: The onset and interannual variability of the Asian summer monsoon in relation to land-sea thermal contrast. *J. Climate*, **9**, 358−375.

Li, Z., and L. Zhang, 2009: Wind onset and withdrawal of Asian summer monsoon and their simulated performance in AMIP models. *Clim. Dyn.*, **32**, 935−968.

Meehl, G. A., C. Covey, T. Delworth, M. Latif, B. McAvaney, J. F. B. Mitchell, R. J. Stouffer, and K. E. Taylor, 2007: The WCRP CMIP3 multimodel dataset: A new era in climate change research. *Bull. Amer. Meteor. Soc.*, **88**, 1383−1394.

Murakami, T., and J. Matsumoto, 1994: Summer monsoon over the Asian continent and western North Pacific. *J. Meteor. Soc. Japan*, **72**, 719−745.

Richter, I., and S.-P. Xie, 2008: Muted precipitation increase in global warming simulations: A surface evaporation perspective. *J. Geophys. Res.*, **113**, D24118, doi:10.1029/2008JD010561.

Santer, B. D., and co-authors, 2005: Amplification of surface temperature trends and variability in the tropical atmosphere. *Science*, **309**, 1551−1556.

Taylor, K. E., 2001: Summarizing multiple aspects of model performance in a single diagram. *J. Geophys. Res.*, **106**, 7183−7192.

Ueda, H., 2005: Air-sea coupled process involved in stepwise seasonal evolution of the Asian summer monsoon. *Geogr. Rev. Japan*, **78**, 825−841.

Ueda, H., and T. Yasunari, 1998: Role of warming over the Tibetan Plateau in early onset of the summer monsoon over the Bay of Bengal and the South China Sea. *J. Meteor. Soc. Japan*, **76**, 1−12.

Ueda, H., T. Yasunari, and R. Kawamura, 1995: Abrupt seasonal change of large-scale convective activity over the western Pacific in the northern summer. *J. Meteor. Soc. Japan*, **73**, 795−809.

Ueda, H., A. Iwai, K. Kuwako, and M. E. Hori, 2006: Impact of anthropogenic forcing on the Asian summer monsoon as simulated by eight GCMs. *Geophys. Res. Lett.*, **33**, L06703, doi:10.1029/2005GL025336.

Uppala, S. M., and co-authors, 2005: The ERA-40 re-analysis. *Quart. J. Roy. Meteor. Soc.*, **131**, 2961−3012.

Wang, B., Q. Ding, X. Fu, I.-S. Kang, K. Jin, J. Shukla, and F. Doblas-Reyes, 2005: Fundamental challenge in simulation and prediction of summer monsoon rainfall. *Geophys. Res. Lett.*, **32**, L15711, doi:10.1029/2005GL022734.

Webster, P. J., and S. Yang, 1992: Monsoon and ENSO: Selectively interactive systems. *Quart. J. Roy. Meteor. Soc.*, **118**, 877−926.

Xu, K.-M., and K. A. Emanuel, 1989: Is the tropical atmosphere conditionally unstable? *Mon. Wea. Rev.*, **117**, 1471−1479.

Manuscript received 28 February 2011, accepted 24 May 2011
SOLA: http://www.jstage.jst.go.jp/browse/sola